ON THE SENSITIVITY OF A FREE ANNULAR SWIRLING JET TO THE LEVEL OF SWIRL AND A PILOT JET

M. García-Villalba and J. Fröhlich

SFB 606, University of Karlsruhe,
Kaiserstr. 12, 76128, Karlsruhe, Germany

ABSTRACT

The paper presents large eddy simulation of unconfined swirling jets. In the first part, an unconfined annular jet is investigated for swirl numbers ranging from 0 to 1.2. The impact of the swirl on the mean flow and the precessing vortex structures in this flow is analysed. In the second part of the paper, a co-annular pilot jet is introduced near the axis. The investigations show that the additional swirl near the axis has a stronger effect than the pilot jet itself, leading to an almost entire removal of coherent structures.

KEYWORDS

swirling jets, annular jets, large eddy simulation, coherent structures, pilot jet

INTRODUCTION

Swirling flows are widely used in many engineering applications. In combustion devices, they are often used to stabilize the flame by means of a recirculation zone. Swirling flows, however, are prone to instabilities which can trigger pronounced unsteadiness of combustion degrading the performance of the whole system. Lean premixed burners in modern gas turbines often contain a richer pilot flame typically introduced near the axis of the swirl burner raising the question of how this additional jet modifies the fluid mechanical behaviour of the system. This issue is addressed in the present paper for a model system corresponding to an experimental setup.

Swirling flows are difficult to model with Reynolds-averaged methods (Jakirlić *et al.* 2002) due to the effects of streamline curvature of the mean flow. Large eddy simulations (LES) of such flows not encountering this problem such as Wegner *et al.* (2004), Wang *et al.* (2004), etc., are still scarce. The present paper aims at using LES to investigate these flows in a physical perspective and in particular to analyse their large scale instantaneous vortex structures. In García-Villalba *et al.* (2004a, 2005) the present authors performed LES of an unconfined annular swirling jet and validated the simulation method by means of detailed comparisons with experiments for the same configuration. Large scale

coherent helical structures precessing around the symmetry axis at a constant rate were identified in these computations. The first goal of the present paper is to investigate the influence of the swirl parameter on these structures. Second, the impact of an additional co-annular pilot jet near the axis is investigated.

NUMERICAL METHOD

The simulations have been performed with the code LESOCC2 (Hinterberger 2004), which is a successor of the code LESOCC (Breuer & Rodi 1996). It solves the incompressible Navier-Stokes equations on curvilinear block-structured grids. A collocated finite-volume discretization with second-order central schemes for convection and diffusion terms is employed. Temporal discretization is performed with a three-stage Runge-Kutta scheme solving the pressure-correction equation in the last stage only.

The computations for the two issues addressed in this paper have been performed with two very similar configurations. These match two experiments performed by Büchner and Petsch (2004) which are used for validation (the first configuration had also been investigated previously by Hillemanns 1988). For each sensitivity study one of the computations corresponds to an experiment so that these data can be used for comparison. The variation of the swirl number was investigated using the geometry shown in Fig. 1*(a)* with an inner diameter of the annular jet of 0.5*D* where *D* is the outer diameter of the jet. The geometry of the second configuration only differs with respect to the inlet and is detailed below. The rest of the computational domain is the same (Fig. 1*(a)*). The block-structured mesh consists of about 2.5 million cells in both cases. The grid is stretched in both the axial and the radial direction to allow for concentrations of points close to the jet exit and the inlet duct walls, while 100 grid points are used in the azimuthal direction. The stretching factor is everywhere less than 5 %. The minimum axial spacing appears at the jet outlet and is $\Delta x = 0.02\ R$. Close to the walls, the minimum radial spacing is $\Delta r = 0.012\ R$. In the first part of the paper, the subgrid-scale model used is the Smagorinsky model with Van Driest damping and a model constant C_s=0.1. In the second part, the dynamic model of Germano *et al.* (1991) has been employed, with least squares averaging and three-dimensional test filtering. The eddy viscosity in the latter case is smoothed by temporal relaxation. In what follows, *R=D/2* is the reference length and capital letters are used throughout the paper to indicate values averaged in time and circumferential direction.

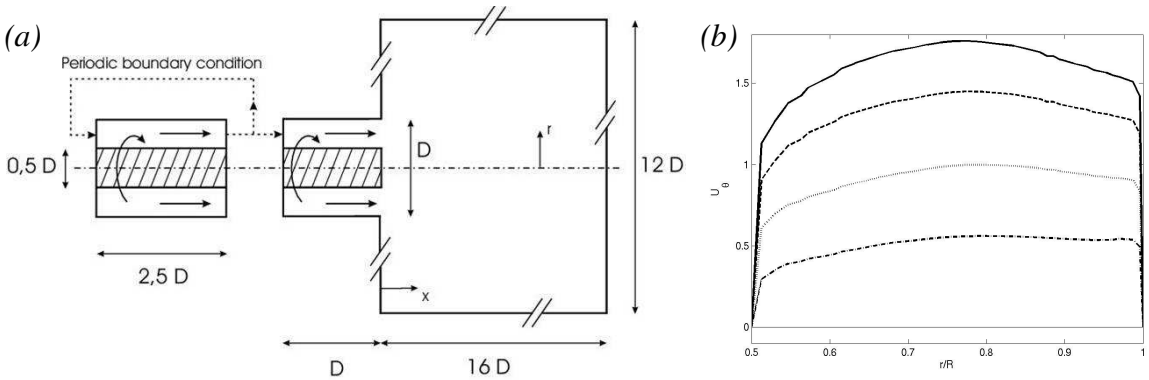

Figure 1: *(a)* Sketch of the computational domain and boundary conditions for the swirl study. *(b)* Inflow conditions. Mean tangential velocity imposed at *x/R*=-2. The line styles are defined in Table 1.

The inflow conditions are obtained by performing simultaneously a separate periodic LES of swirling flow in an annular pipe using body forces to impose swirl and flow rate as described in Pierce & Moin (1998). This approach is illustrated in Fig. 1*(a)* and has been validated in García-Villalba *et al* (2004b). No-slip boundary conditions are applied at the walls. The entrainment of outer fluid into the jet is

simulated using a weak co-flow in the outlet plane x/R=0 remote from the jet. Free-slip conditions are applied at the open lateral boundary which is placed far away from the region of interest (see Fig. 1*(a)*). A convective outflow condition is used at the exit boundary.

SENSITIVITY TO THE LEVEL OF SWIRL

An overview of the simulations performed is shown in Table 1. The Reynolds number of the flow based on the bulk velocity U_b=25.5 m/s and the outer radius of the jet R=50 mm is Re=81500. The swirl parameter is defined at the inflow plane x/R = -2 as

$$S = \left(\int_0^R \rho u w r^2 \mathrm{d}r \right) / \left(R \int_0^R \rho u^2 r \mathrm{d}r \right) \tag{1}$$

where u and w are the axial and azimuthal velocities, respectively. The range covered by the simulations is very wide, including a simulation without swirl, Sim. 1, another with a low level of swirl, Sim. 2, and three simulations with a high level of swirl, Sims. 3,4,5.

TABLE 1

OVERVIEW OF THE SIMULATIONS PERFORMED TO INVESTIGATE THE IMPACT OF THE SWIRL NUMBER

Simulation	1	2	3	4	5
Swirl number S	0	0.4	0.7	1	1.2
Line style	solid (thin)	dashed-dotted	dotted	dashed	solid (thick)

Fig. 1*(b)* addresses the inflow conditions for the main simulation imposed at x/R=-2. It shows the mean azimuthal velocity resulting from imposing the desired swirl number in the precursor simulation. In fact, the mean azimuthal velocity increases with S, while the mean axial velocity (not shown here) is almost unchanged in all cases.

Streamlines

First of all, a general view of the flow is presented. Fig. 2 shows the time-averaged streamlines computed from four of the simulations in Table 1. As the jet is annular, the flow characteristics differ from those of a usual round jet. In the non-swirling case, Fig. 2*(a)*, a geometry-induced recirculation zone (GRZ) is formed due to the bluff-body effect of the cylindrical centre body. Fig. 2*(b)* shows the case of low swirl, Sim. 2. In this case, additional to the GRZ, a very thin central recirculation zone (CRZ) appears close to the axis. It extends up to about x/R=4. For this level of swirl, no CRZ is expected in a round jet (Gupta *et al* 1984), but in the present case the cylindrical center body introduces this feature. Increasing S leads to an increase in the size of the CRZ. For S=0.7, Fig. 2*(c)*, the length of the CRZ is about 4R, and its width is increased to 0.6R, attained at x/R=2. The GRZ is still present at this level of swirl but substantially reduced in size and strength. For S=1, not shown here, the CRZ is longer reaching until x/R=8 and attaining its maximum width of 0.8R at x/R=1.5, i.e. further upstream compared to Sim. 3. Finally, Fig. 2*(d)* shows the case S=1.2, in which the CRZ has reached x/R=0, and the GRZ has been merged into the CRZ. The length of the CRZ is about 10R and the maximum width of 0.8R is attained at x/R=1. Fig. 2 shows that with increasing swirl number the jet spreads further outwards in radial direction and the strength of the CRZ increases substantially. Let us finally address the slope of the streamlines in Fig. 2 remote from the jet, starting at x/R=0 and r>R. Their shape is due to the co-flow boundary condition. Note, however, that the velocity at this location is only 5% of the jet axial velocity, so that the influence on the region of interest is negligible, as will

be seen in Figs. 3 and 4. This was also checked with different amounts of co-flow in García-Villalba *et al.* (2005).

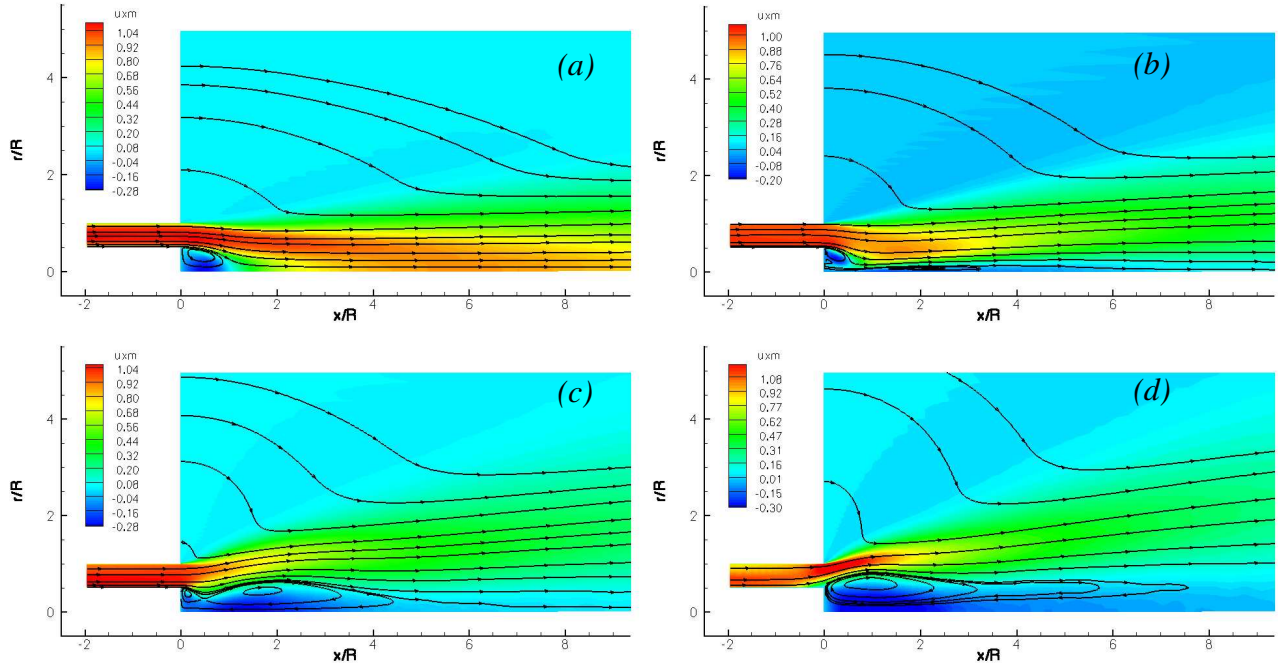

Figure 2: Streamlines of the average flow. *(a)* Sim 1. *(b)* Sim 2. *(c)* Sim 3. *(d)* Sim 5.

Mean Flow and Statistics

Experimental data were available only for one flow condition, equivalent to S=1.2. The comparison of experiment and simulation was performed in García-Villalba *et al.* (2004a) and is not repeated here. The agreement between experiment and simulation is excellent. Figs. 3 and 4 show mean velocity and turbulent intensity profiles at two axial positions in the near flow field of the jet. Fig. 3 shows profiles very close to the jet exit at x/R=0.2. Here, the jet forms two complex three-dimensional shear layers, the inner one with the recirculation zone, and the outer one with the surrounding co-flow. At this position, x/R=0.2, the inner one increases in thickness with S, reaching 0.5R for S=1.2, while the outer one remains thin and is just displaced radially outwards with increasing S. The axial fluctuations in Fig. 3*(c)* exhibit a peak in the region of the shear layer. The thicker the shear layer, the more pronounced and wider is the peak. The outer shear layer does not present these variations, but with increasing S, the velocity-difference is larger, and therefore the turbulence intensity is also larger. The velocity difference is generated by both axial and azimuthal velocity and hence complemented by Fig. 3*(b)* showing mean tangential velocity profiles. Similar conclusions as for the axial fluctuations hold for the azimuthal ones in Fig. 3*(d)*.

Fig. 4 shows the same quantities as Fig. 3 but at x/R=3. This position is located within the CRZ in the simulations with swirl. A qualitative difference between the simulations with $S \leq 0.4$ and the simulations with $S \geq 0.7$ is observed in all data. The spreading and decay rate is much lower in the former, Fig. 4*(a)*. The profiles of mean velocity and fluctuations in Sims 3-5 do not present substantial differences at this location, i.e. as soon as the swirl is high enough to produce a strong recirculation zone, a kind of saturation of the profiles is reached. The shape of the turbulent intensities is also the same, Figs. 4*(c)* and 4*(d)*, with a slight increase of intensity with S. At this position, the distinction between shear layers is not reflected by the profiles of the fluctuations. Only for the two low swirl cases, it is still possible to distinguish the peaks due to the fact that these flows develop slower in space than the others.

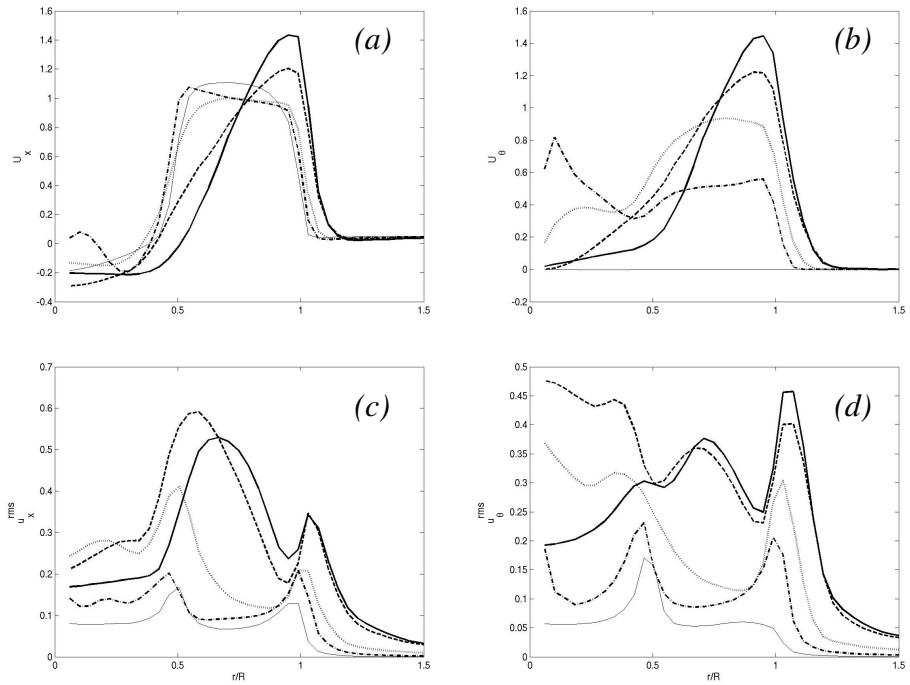

Figure 3: Profiles at *x/R*=0.2 *(a)* Mean axial velocity. *(b)*Mean tangential velocity. *(c)* RMS values of axial velocity. *(d)* RMS values of tangential velocity. The line styles are defined in Table 1.

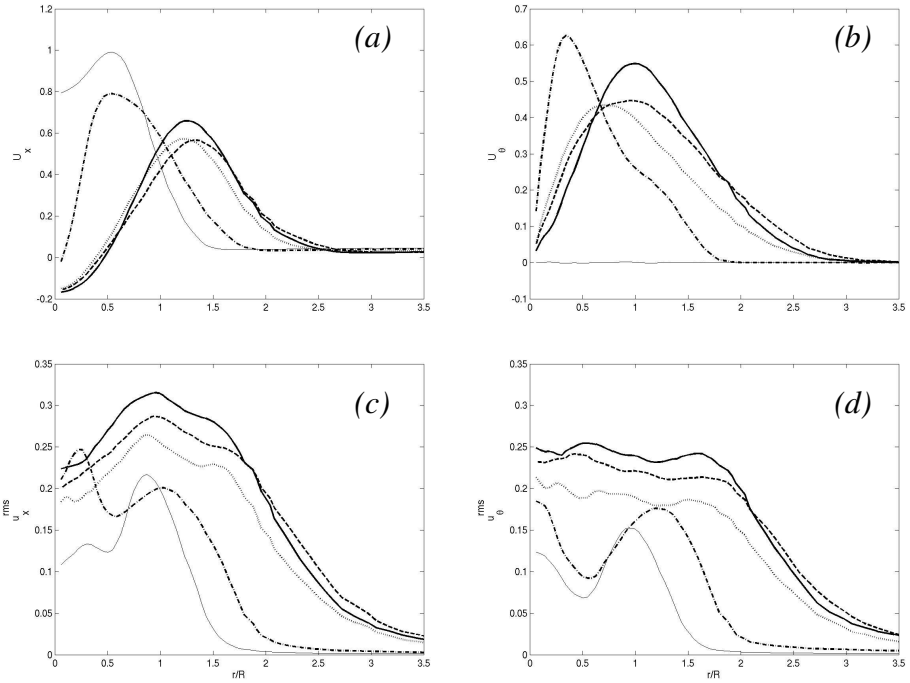

Figure 4: Profiles at *x/R*=3 *(a)* Mean axial velocity. *(b)*Mean tangential velocity. *(c)* RMS values of axial velocity. *(d)* RMS values of tangential velocity. The line styles are defined in Table 1.

Flow visualization and Spectra

In García-Villalba *et al.* (2005) large scale coherent structures were identified and their evolution and interaction described for a high swirl number case, equivalent to Sim. 5. It was shown that two families of structures appear, which are best visible in Fig. 5*(b)*. The outer, spiralling structure is located in the outer shear layer, see Fig. 3*(a)*, where $\partial U_x / \partial r < 0$, the darker one in the inner shear layer between the

annular jet and the recirculating fluid, where $\partial U_x / \partial r > 0$. In the cited reference it has been shown that these structures result from Kelvin-Helmholtz instabilities as they are perpendicular to the average streamlines. It is now interesting to study how these structures are modified when varying the swirl number. This is reported in Fig. 5. Due to lack of space, only one snapshot is included but further views and animations were produced upon which the following comments are based. In the literature on the subject the inner structure is usually called 'precessing vortex core' (PVC), (Gupta *et al* 1984). In the case of low swirl, it is not expected to be observed. However, as in the present case a very thin CRZ is produced, a thin elongated structure can be seen in Fig. 5*(a)*. Larger values of $p'<0$ do not show any larger scale structure in these data. In the case of strong swirl the structures mentioned above are observed. For S=0.7, a single inner and a single outer structure are present. Animations of the flow show that their rotation is in phase and very regular. Upon increasing S, Figs. 5*(c)* and 5*(d)*, the irregularity of the flow grows in the sense that the PVC change in number during their evolution and for S=1.2, up to three of them can co-exist at certain instants. Furthermore, with increasing S, the inner structures enter the inlet duct, slightly for S=1, and in a more pronounced way for S=1.2. At the same time the PVC is displaced off the symmetry axis since the shear layers are shifted outwards as discussed above. As a consequence, the tangential fluctuations near the axis increase for S=0 to S=1 while decreasing for the larger value S=1.2. The radial fluctuations behave similarly.
The outer structures consist of a long spiral for S=0.7 and also become more irregular with increasing S. Another interesting feature is that the separation between the inner and the outer structures decreases with increasing S, to the point that in absence of colour it is difficult to distinguish them when S=1.2. The reason for this behaviour is that the two shear layers, identified as the origins and locations of both types of structures, approach each other with increasing S, as seen in Fig. 3*(a)*.

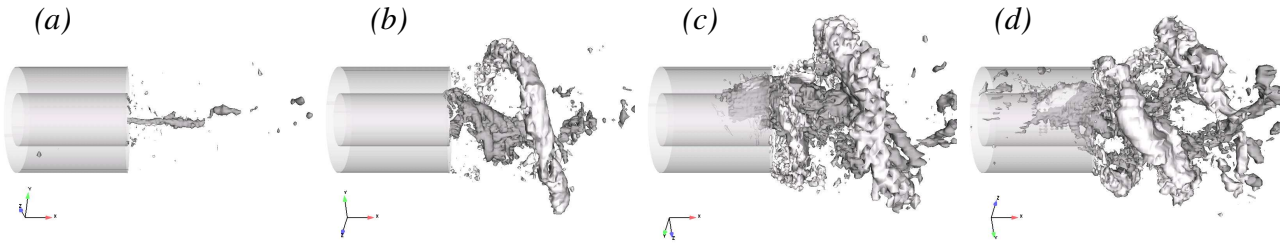

Figure 5: Instantaneous coherent structures visualized using an iso-surface of the instantaneous pressure deviation $p'=p-P=$ - 0.2 . *(a)* Sim 2. *(b)* Sim 3. *(c)* Sim 4. *(d)* Sim 5. The colour is computed according to the sign of the radial gradient of the mean axial velocity.

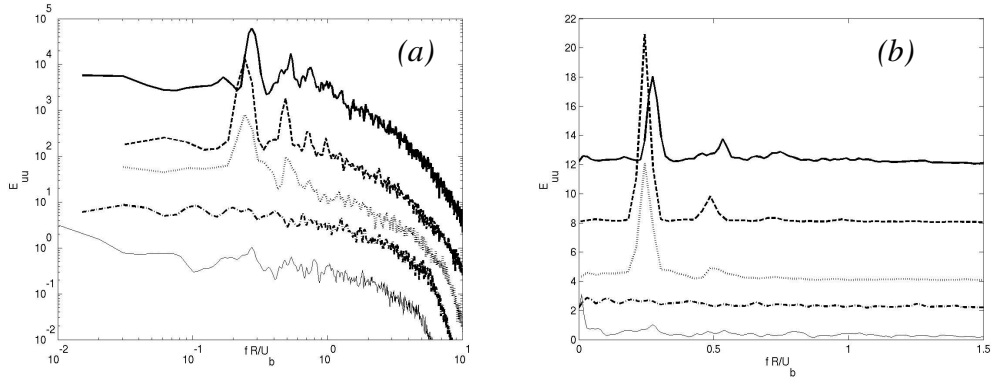

Figure 6: PSD of axial velocity fluctuations at x/R=0.1, r/R=0.7. Arbitrary units are used in the vertical axis and the curves have been shifted vertically for readability. *(a)* Diagram with logarithmic axes. *(b)* The same diagram with linear axes. The line styles are defined in Table 1.

Fig. 6 shows the power spectrum density (PSD) of axial velocity fluctuations at x/R=0.1, r/R=0.7, i.e. very close to the jet exit and in the region of the inner shear layer for all cases. In the cases of low swirl the spectra do not show a pronounced peak. When the level of swirl is high, i.e. $S \geq 0.7$, a dominant

peak and its higher harmonics appear in the spectrum. This peak reflects the precessing structures observed in Figs. 5(b)-5(d) (García-Villalba *et al.* 2004a). For S=0.7 and S=1, the same frequency f_{peak} = 0.24 U_b/R is observed, changing only slightly to f_{peak} = 0.28 U_b/R for S=1.2. Note that although the mean tangential velocity increases by about U_b in the inlet section (Fig. 1*(b)*), this increase is reduced near the outlet of the annular pipe (Fig. 3*(b)*) and further downstream (Fig. 4 *(b)*). Nevertheless, the fact that f_{peak} does not change much with S over a broad range is an important result of the present study.

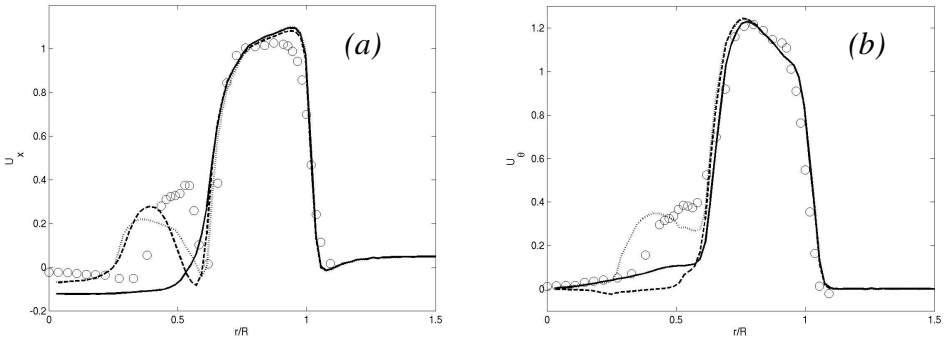

Figure 7: Profiles of mean velocity at x/R=0.1 *(a)* Mean axial velocity. *(b)* Mean tangential velocity. The line styles are defined in Table 2.

INFLUENCE OF A PILOT JET

Configuration

In the second part of the paper, the effect of an additional inner jet is studied. The inflow part of this configuration differs from the one described in Fig. 1 while the rest of the computational domain is identical. Here, the precursor simulation for the main annular jet is replaced by a duct reaching to x=-3.82R and bending radially outwards to r=2.18R. At this position, where in the experiment the radial swirl generator is located, steady swirling flow is imposed in the simulations. It undergoes a rapid pseudo-transition and reproduces the experimental profiles of the main jet in the plane near the outlet quite well (cf. Fig. 7 below), provided that the swirl is adjusted appropriately. This procedure was studied and compared to the one of the previous section in García-Villalba *et al.* (2004b). To allow comparison with the simulations of the previous section, the resulting swirl number in the main jet at x=-2R, has been determined. Its value is S=1.05. In the experiment, a co-annular pilot jet was introduced featuring an axial swirl generator ending flush with the outlet plane at x=0. This jet is modelled with a precursor simulation similar to Fig. 1 which also ends at x=0. The direction of swirl is co-rotating with the main jet. In this configuration the inner and outer diameter of the pilot jet is 0.27D and 0.51D, respectively, while the inner and outer diameter of the main jet is 0.63D and D, respectively. The flow conditions are very similar to the previous ones. The Reynolds number based on the bulk velocity of the main jet only U_b=22.1 m/s and the outer radius of the jet R=55 mm is Re=81000 while the swirl number at x=-2R is almost exactly the same as for Sim 4. The different width of the main jet, however, precludes direct comparison with the above computations. The mass flux of the pilot jet is 10% of the total mass flux and the swirl number for the pilot jet alone is 1.

TABLE 2

OVERVIEW OF THE SIMULATIONS PERFORMED TO INVESTIGATE THE INFLUENCE OF A PILOT JET

Simulation	6	7	8	Exper.
Inner jet	No	Yes	Yes	Yes
Inner jet with swirl	-	No	Yes	Yes
Line style	solid	dashed	dotted	O

The purpose of these simulations is to clarify the impact of the inner jet on the stability of the entire flow. This is investigated by consideration of three cases which are summarized in Table 2. Fig. 7 shows the mean axial and azimuthal velocity profiles near the outlet at x/R=0.1 for the three cases, in order to visualize the strength of the pilot jet. The deviation with respect to the experimental data in this range results from the model for the pilot jet. Its inflow condition is imposed at x=0, while in the experiment the flow is less stiff. Moreover, the guide vanes of the axial swirl generator are not represented since this renders grid generation very complicated. Nevertheless, the present data allow very well to assess the impact of the pilot jet on the flow as will be demonstrated below.

Mean flow

The streamlines for the three cases investigated are displayed in Fig. 8. Since S is in the range of high swirl, the flow is very similar to the ones in the previous section. Fig. 8*(a)* showing the case without pilot jet indeed is very close to Fig. 2*(d)*. As before, a CRZ starting directly behind the cylindrical centre body occupies a long region near the symmetry axis. The streamlines with pilot jet of Sim 7 in Fig. 8*(b)* are very close to those of Sim 6, with just the streamlines emanating from the pilot jet entering the inner shear layer. In the case of the swirled pilot jet, Sim 8, the shape of the recirculation zone is slightly modified in the region of its maximum width but still remains mostly unchanged. Fig. 9 presents a comparison of velocity profiles at x/R=3 from the simulations together with experimental data. Fig. 7, 8, and 9 show that the influence of the pilot jet on the average flow is only small.

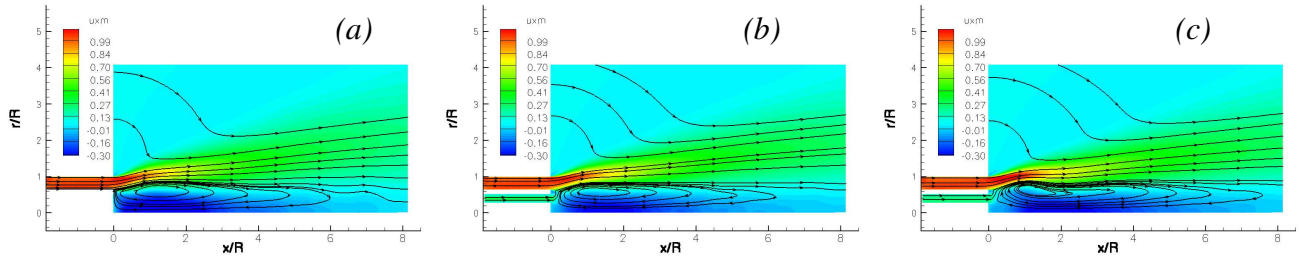

Figure 8: Streamlines of the average flow. *(a)* Sim 6. *(b)* Sim 7. *(c)* Sim 8.

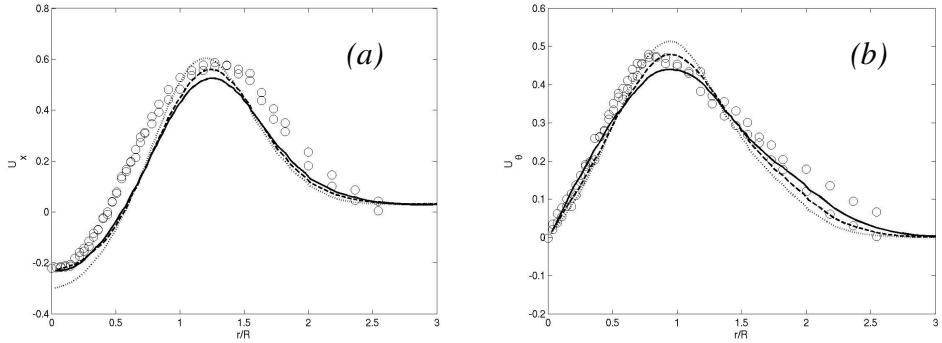

Figure 9: Profiles of mean velocity at x/R=3. *(a)* Mean axial velocity. *(b)* Mean tangential velocity. The line styles are defined in Table 2.

Flow visualization and Spectra

The instantaneous flow is now visualized in exactly the same way as in the previous section using iso-surfaces of pressure fluctuations, Fig. 10. Obviously, there are important differences between the three cases. Without pilot jet, Fig. 10*(a)*, the structures have the characteristics described in the first part of the paper. They are very coherent, precess at a quasi-regular rate and persist over long time intervals. When the non-swirled pilot jet is introduced, Fig. 10*(b)*, it is still possible to recognize similar structures as in the case without pilot jet. These are however substantially less coherent, much thinner,

and do not persist that long. In particular, the PVC are smaller and are more numerous along the circumference. In this case, four or five small PVC can co-exist at certain instants. Finally, the addition of swirl to the pilot jet has a dramatic impact on the flow, Fig. 10*(c)*. The regularity is completely lost and the appearance of the structures is more random. Here, even the outer structures are affected and have almost vanished or, when they appear, exhibit only small coherence The addition of near-axis swirl hence is observed to have a strong influence on the instantaneous flow characteristics. Recently, in a different context, the addition of near axis swirl has been proposed as a strategy to control vortex breakdown, Husain *et al.* (2003).

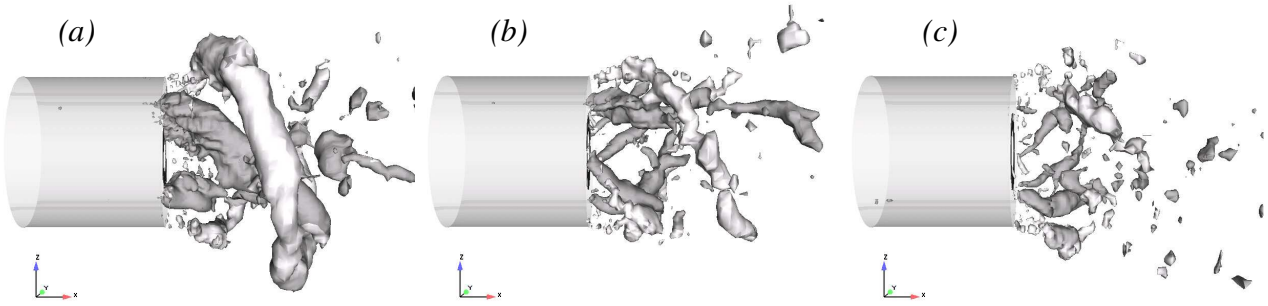

Figure 10 : Instantaneous coherent structures visualized using an iso-surface of the instantaneous pressure deviation $p'-\langle p\rangle = -0.2$. *(a)* Sim 6. *(b)* Sim 7. *(c)* Sim 8. Colour is given by the sign of the radial gradient of the mean axial velocity.

The previous analysis of the coherent structures is confirmed by analysing the PSD of the radial velocity fluctuations at two points close to the outlet at x/R=0.4. Fig. 11(a) shows this data on the symmetry axis. Note that in spite of the difference in geometry with respect to the configuration studied in the previous section, the peak in the spectrum for Sim. 6 also appears at a frequency f_{peak} = 0.24 U_b/R. The difference in geometry hence does not have much influence in the precessing rate of the structures. A pronounced peak can also be observed for Sim. 7. The spectrum of Sim. 8 also shows a peak but at substantially larger time scales. These are hardly resolved by the present integration time and deserve further investigation. Fig. 11*(b)* shows the PSD at r/R=0.6, i.e. in the inner shear layer of the main jet. The spectrum of Sim. 6 shows a pronounced first and second harmonic (both label A). The spectrum of Sim. 7 also exhibits peaks at these frequencies, but their energy content is smaller. Instead, more energy is displaced to the next harmonic, which shows that the PVC are more irregular in this case. For Sim. 8 the energy is contained in substantially higher harmonics (the most dominant ones with label B) and much less in low-frequency modes.

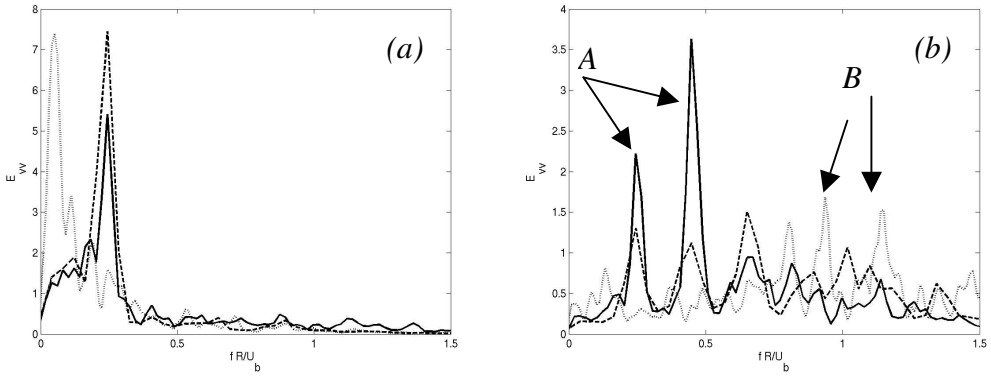

Figure 11: PSD of radial velocity fluctuations at x/R=0.4. *(a)* location on the symmetry axis, r/R=0. *(b)* r/R=0.6. The line styles are defined in Table 2.

CONCLUSIONS

The computations performed for an annular jet show dominating spiralling structures in the two shear layers present in this flow. With increasing swirl number and S beyond 0.7, with the definition employed here, their shape becomes more complex but the precessing frequency remains almost constant over a wide range. When a pilot jet is introduced close to the axis the average flow is only little affected. Visualizations and spectra however demonstrate that although axial and angular momentum of this jet are small, it has a dramatic effect on the instantaneous vortex structures. This is an important result for the consideration of mixing effects in this type of flow. Based on the data presented here more analyses of the flow field will be performed in the future. It would also be interesting to further modify the parameters of the pilot jet and, e.g., investigate the consequences of counter-rotating swirl.

ACKNOWLEDGEMENTS

The authors gratefully acknowledge the support of the German Research Foundation (DFG) through the collaborative research center SFB 606 'Unsteady Combustion'. The calculations were performed on the IBM Regatta of the Computing Center of Garching (RZG) and on the VPP5000 of the Forschungszentrum Karlsruhe (FZK).

REFERENCES

Breuer M. and Rodi W. (1996). Large eddy simulation of complex turbulent flows of practical interest, In Hirschel E. (ed.), *Flow simulation with high performance computers II*, vol 52 of *Notes on Numerical Fluid Mechanics*, pages 258-274. Vieweg, Braunschweig, Germany.

Büchner H. and Petsch O. (2004). Private communication.

García-Villalba M., Fröhlich J. and Rodi W. (2004a). Unsteady phenomena in an unconfined annular swirling jet. In Andersson H.I. and Krogstad P.Å. (eds.) *Advances in Turbulence X*. 515-518. Cimne, Barcelona, Spain.

García-Villalba M., Fröhlich J. and Rodi W. (2004b). On inflow boundary conditions for large eddy simulation of turbulent swirling jets. In *Proc. 21st Int. Congress of Theoretical and Applied Mechanics*. Warsaw. Poland.

García-Villalba M., Fröhlich J. and Rodi W. (2005). Large eddy simulation of the near field of a turbulent unconfined annular swirling jet. In preparation

Germano M., Piomelli U., Moin P. and Cabot W. (1991). A dynamic subgrid-scale eddy viscosity model. *Phys. Fluids A*, **3**, 1760-1765

Gupta A.K., Lilley D.G. and Syred N. (1984). *Swirl Flows*, Abacus Press, Kent, USA.

Hinterberger C. (2004). Dreidimensionale und tiefengemittelte Large-Eddy-Simulation von Flachwasserströmungen. PhD thesis, University of Karlsruhe.

Hillemanns R. (1988). Das Strömungs und Reaktionsfeld sowie Stabilisierungeigenschaften von Drallflamen unter dem Einfluss der inneren Rezirkulationszone. PhD thesis, University of Karlsruhe.

Husain H.S., Shtern V. and Hussain F. (2003). Control of vortex breakdown by addition of near-axis swirl. *Phys. Fluids* **15:2**, 271-279

Jakirlić S., Hanjalić K. and Tropea C. (2002). Modeling rotating and swirling turbulent flows: a perpetual challenge. *AIAA J.* 40:10, 1984-1996

Pierce C.D. and Moin P. (1998). Method for generating equilibrium swirling inflow conditions. *AIAA J.* **36:7**,1325-1327

Wang P., Bai X.S., Wessman M. and J. Klingmann (2004). Large eddy simulation and experimental studies of a confined turbulent swirling flow. *Phys. Fluids* **16:9**, 3306-3324

Wegner B., Kempf A., Schneider C., Sadiki A., Dreizler A. and Janicka J. (2004) Large eddy simulation of combustion processes under gas turbine conditions. *Prog. Comp. Fluid Dyn.* **4**,257-263